

Optical properties of GaAs/Al_xGa_{1-x}As quantum wells disordered by ion implantation

I. Shtrichman, D. Gershoni, and R. Kalish

Department of Physics and Solid State Institute, Technion-Israel Institute of Technology, Haifa 32000, Israel

(Received 20 March 1997)

Photoluminescence, photoluminescence excitation, and time-resolved optical spectroscopy are used to study ion-induced disordered GaAs/Al_xGa_{1-x}As quantum wells. The experimental data are used to quantify the structural modifications of the implanted quantum wells after they are thermally annealed. We show that a finite density of nonradiative traps, associated with the Al atoms which diffused into the GaAs quantum well during the annealing process, is responsible for the quantum wells' photoluminescence quenching. We use a simple vacancy controlled diffusion mechanism to model the ion-induced structural modification and its dose dependence. Our model explains the ratio between the interface diffusion length (~ 10 Å) and the lateral extent of the intermixing around each traversing ion track (~ 200 Å). It fails, however, to predict the correct dependence of the interface diffusion length on the implantation dose. [S0163-1829(97)06228-0]

I. INTRODUCTION

Semiconductor heterostructure interface intermixing using ion implantation followed by thermal annealing is an important tool in modern science and technology.^{1,2} In particular, this tool is used as an important avenue towards the fabrication of lower dimensionality quantum structures such as quantum wires^{3,4} and quantum dots.⁴

The technique combines two main stages: First, selective areas of the heterostructured sample are implanted with high-energy ions using either focused ion beams,⁵ or by implantation through lithographically defined metal mask.⁶ Second, the implanted sample undergoes thermal annealing, during which its temperature is sharply increased, and enhanced implantation-induced diffusion of the structure interfaces takes place due to defects which were generated by the traversing ions. Recent studies using high-resolution transmission electron microscopy and chemical lattice imaging of unannealed implanted heterostructures show that the lateral extension of the implantation-induced damage is 20–50 Å around a single-ion track, depending on the ion kinetic energy, its mass, and the mass of the heterostructure atoms.⁷ This is in agreement with Monte Carlo simulations of the implantation process.⁸ The lateral extent of the ion-induced interface diffusion and disordering during the annealing stage, however, is found to be much longer. Recent photoluminescence (PL) experiments estimate the range of the affected region after the heat treatment to be as large as 200 Å in GaAs/Al_xGa_{1-x}As heterostructures^{9,10} and as large as 2000 Å in In_xGa_{1-x}As/GaAs structures.¹¹

The ion-induced damage to the lattice, which results in a drastic reduction of its optical quality, is mostly recovered after the heat treatment, and the heterostructures usually resume their optical efficiency. Indeed, optical characterization techniques such as PL,^{10,11} and cathodoluminescence⁵ were extensively used for the study and assessment of the structural modifications of ion implanted and thermally annealed semiconductor heterostructures. Yet, these optical techniques are limited since they monitor only the lowest-energy state of the excited charge carriers.

In this study we report on optical studies of ion-implanted

and rapid thermally annealed single GaAs/Al_xGa_{1-x}As quantum wells (QW's). We used in a combined manner PL, photoluminescence excitation (PLE) and time-resolved spectroscopy in order to quantify the structural modifications that these wells undergo, and to characterize the change in their optical properties as a function of the implantation dose.

We show that implantation-induced interdiffusion of the QW's interfaces results in significant blueshifts of the optical transitions between confined levels of carriers in these wells. From the ground- and excited-states transition energies we gain information on the potential profile that carriers within the QW are subjected to, and thus relate this profile to the ion-implantation dose. We infer the spatial extent of the interdiffused QW interfaces and hence the density of redistributed Al atoms, and their dependence on the implantation density. We account for the ratio between the interfaces diffusion length (~ 10 Å) and the lateral intermixing radius (~ 180 Å), using a simple vacancy assisted diffusion model. From the temperature, well dimension, and implantation dose dependence of the PL efficiency and its decay time we conclude that a deep nonradiative trap associated with the Al atoms is responsible for the reduction of the optical efficiency of these implanted heterostructures.

The work is organized as follows: In Sec. II we describe the experimental setup and the samples. In Sec. III we outline our experimental findings. In Sec. IV we discuss and analyze the experimental results, and a short summary is presented in Sec. V.

II. EXPERIMENT

The samples were grown by molecular-beam epitaxy on a (100) oriented semi-insulating GaAs substrate. They consisted of five single GaAs QW's of nominal width $L_z=200, 100, 70, 50,$ and 35 Å. The QW's, which were grown at this order, were separated apart by 150-Å-thick barrier layers of Al_{0.3}Ga_{0.7}As. The growth sequence was terminated by a 100-Å thick layer of GaAs in order to prevent oxidation.

After growth the samples were divided into small square pieces of roughly 1 cm² each. Half of each piece was then

implanted with 8-MeV Bi^+ ions in the dose range $N_1 = 2.5 \times 10^{10} - 4 \times 10^{12} \text{ cm}^{-2}$, while the second half of the piece was shielded from the ion beam to serve as an unimplanted reference. With these high-energy implants (projected range: $1.19 \mu\text{m}$) only a negligible fraction of the Bi ions stops in the QW's region which have a total thickness of only $0.15 \mu\text{m}$. Thus, one can safely assume that the implantation-induced layer intermixing is entirely due to damage associated with the passage of the ions, i.e., to displaced Al, Ga, and As atoms. Following implantation, the samples were rapidly thermal annealed for 4 min at 900°C in a N_2 environment using a GaAs proximity cap. We note here that similar samples, implantation, and heat treatment conditions were previously used by Kalish *et al.*¹⁰

For the optical studies the samples were mounted in a helium transfer cryostat which allowed temperature variations in the range of 4–300 K. The PL and PLE spectra were excited with normally incident light of an Ar^+ laser pumped Ti-sapphire laser with a typical power density of $\sim 50 \text{ W/cm}^2$. The emitted light was collected in backscattering geometry and was analyzed by a 0.25-m double monochromator followed by a photomultiplier and a conventional lock-in detection technique. The time-resolved PL spectra were excited with a passively mode-locked Ti-sapphire laser with a pulse duration of 2 ps and repetition rate of 76 MHz. An excitation density of $\sim 10^{12} \text{ photons/cm}^2$ per pulse at $\lambda = 707 \text{ nm}$ was used. A cooled microchannel plate photomultiplier together with time correlated single-photon counting electronics were used in this case to detect the emitted light. The system had an overall temporal resolution of $\sim 50 \text{ ps}$.

III. RESULTS

In Fig. 1 we display the low-temperature PL (dashed lines) and PLE (solid lines) spectra of the 100-Å QW for various implantation doses. The spectra are vertically displaced for clarity. The first and second heavy-hole as well as the first light-hole excitonic transitions are marked in the figure by vertical bars. We note that above a critical implantation dose $N_c = 7.5 \times 10^{10} \text{ cm}^{-2}$ the spectral peaks observed both in the PL and PLE spectra gradually move towards higher energies and their width increases. The Stokes shift, which is the energy difference between the 11H excitonic transition observed in PL (emission) and that observed in PLE (absorption) also increases with the implantation dose. The lowest excitonic transitions can no longer be resolved in the PLE spectra at the highest doses. These results are in agreement with previous PL experiments on implanted QW's,^{8,10,11} in which similar shifts and broadening of the peaks were observed.

Figures 2 and 3 display the temperature dependence of the PL decay time and of the spectrally integrated luminescence intensity, respectively, for the unimplanted control QW's. We then turn in Fig. 4 and 5 to study the effects that the ion-implantation related damage has on the PL.

In Fig. 2 we display the temperature dependence of the PL decay time for various unimplanted QW's. Each point in Fig. 2 was obtained from a fit of a single exponential decay model, convoluted with the system response function, to the measured intensity of the PL signal as a function of time

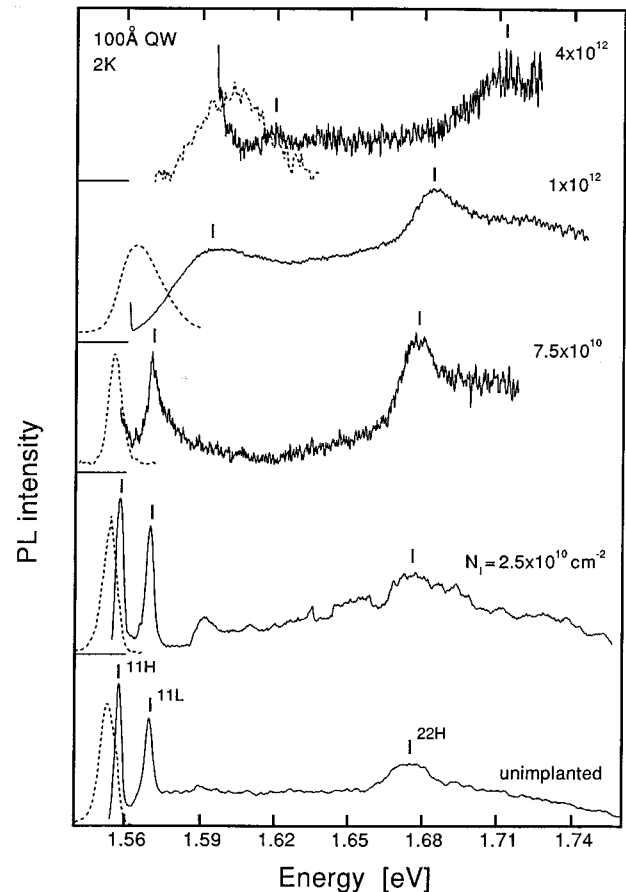


FIG. 1. Low-temperature PL (dashed lines) and PLE (solid lines) spectra of the 100-Å QW for various implantation doses. The vertical bars indicate the observed excitonic peaks.

after the pulsed excitation. The solid lines in the figure represent a theoretical model to be discussed later. In Fig. 3 we display the spectrally integrated PL intensity as a function of temperature for the same unimplanted QW's. Each data point in Fig. 3 represents the spectrally integrated intensity of the PL as measured under the constant density of continuous wave (cw) excitation. It is clearly seen that starting from a certain temperature, which increases with the well width, nonradiative processes take over and the PL efficiency gradually decreases. The solid lines in the figure are fits using the same theoretical model used in Fig. 2.

In Fig. 4 we show the temperature dependence of the PL decay time of the 100- (a) and 70-Å (b) QW's for various implantation doses. For all the implanted QW's a clear trend is noticed in Fig. 4: As the implantation dose increases, the PL decay time reaches its maximum at a lower critical temperature. At temperatures higher than this dose dependent critical temperature, the PL decay time deviates from that of the unimplanted QW as it turns to be almost temperature independent. The solid lines in Fig. 4 represent the same theoretical model as in Figs. 2 and 3. Here, however, we consider in addition an implantation-induced nonradiative trap, as will be described later.

In Fig. 5 the spectrally integrated PL intensity of the 100- (a) and 70-Å (b) QW's, implanted with $7.5 \times 10^{10} \text{ cm}^{-2}$ Bi ions (open circles), is compared with that of the unimplanted QW (full squares). The PL intensities are displayed in the

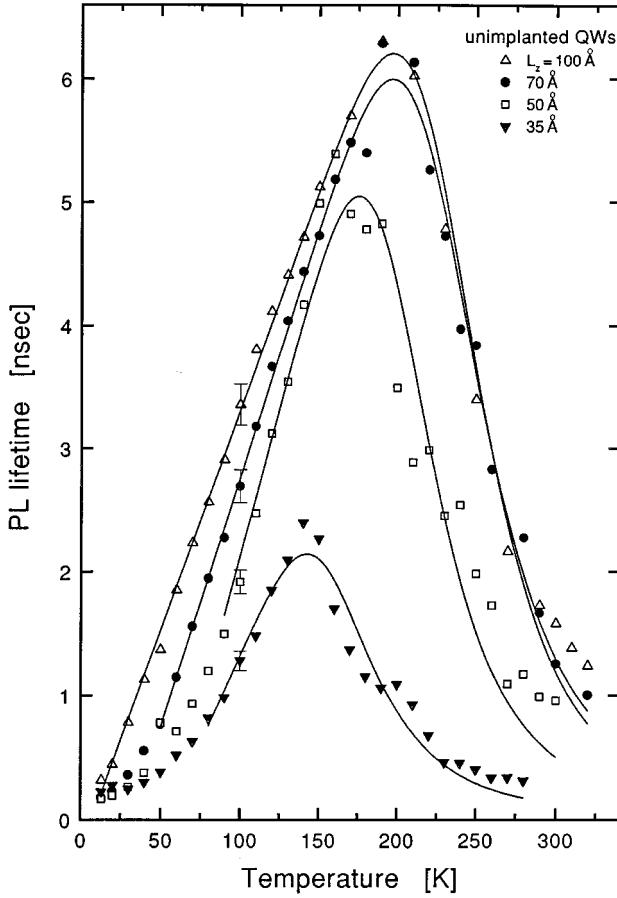


FIG. 2. PL decay time as a function of temperature for various unimplanted QW's. The solid curves represent best fits to the experimental data, using the model as discussed in the text.

figure as a function of the lattice temperature. The critical temperatures for this dose, as deduced from Fig. 4, are marked by the dashed vertical lines. We note that above the critical temperature, the PL intensity of the implanted QW turns weaker as compared to that of the unimplanted one. This behavior clearly indicates that an implantation-induced nonradiative recombination channel is responsible for both the shortening of the excited carrier population lifetime and the reduction in the efficiency of the radiative recombination. The model that quantitatively accounts for the experimental data presented in Figs. 1–5 is described in the discussion below.

IV. DISCUSSION

The ion-implantation related damage and the following thermal annealing, induce layer intermixing and therefore modifications to the initial QW potential structure. The vacancy assisted diffusion of the GaAs/Al_xGa_{1-x}As interface can be described by the following differential equation:¹²

$$\frac{\partial M}{\partial t} = D_v (V \nabla^2 M - M \nabla^2 V), \quad (1)$$

where $M = A - X$ and A , X , V are the probabilities of finding a Ga atom, Al atom, and a vacancy in a group-III lattice site, respectively. D_v is the vacancy diffusion constant, and we

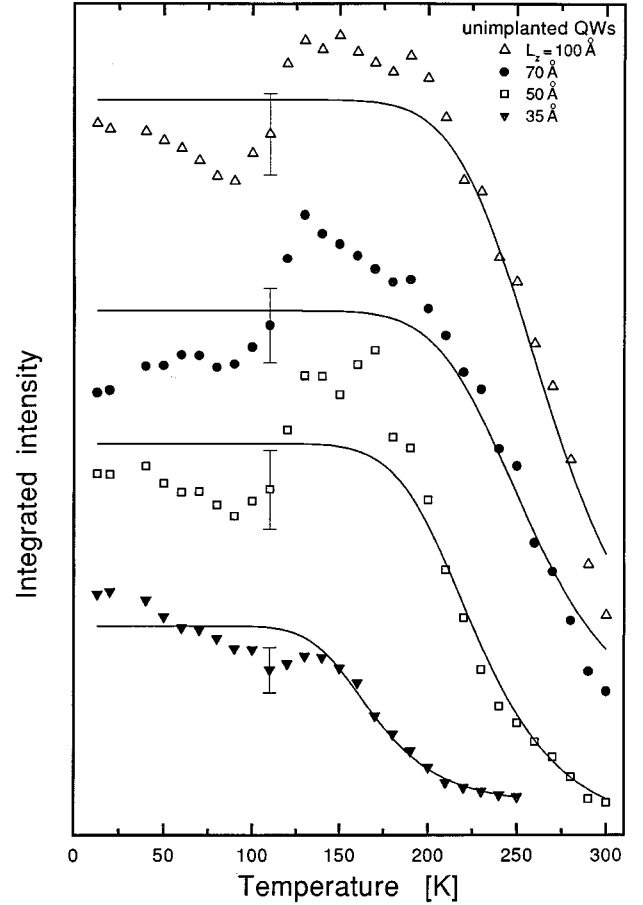


FIG. 3. Temperature dependence of the spectrally integrated PL intensity for various unimplanted QW's. The solid curves represent best fits to the experimental data, using the same model as in Fig. 2.

assume an identical diffusion rate for both Ga and Al. The vacancy diffusion process during the thermal annealing is described in our model by the equation:

$$\frac{\partial V}{\partial t} = D_v \nabla^2 V - \frac{V}{\tau_v}, \quad (2)$$

where τ_v is the vacancy lifetime.

A simple solution to these coupled differential equations can be readily found if one assumes that the vacancies are uniformly distributed after the implantation $V(\mathbf{r}, 0) = V_0$ and that the annealing time is much longer than τ_v . Subjected to these conditions, the following profile for the Al atoms is obtained:¹³

$$X(z) = X_0 \left[1 - \frac{1}{2} \operatorname{erf} \left(\frac{\frac{1}{2} L_z - z}{2 \Delta_i} \right) - \frac{1}{2} \operatorname{erf} \left(\frac{\frac{1}{2} L_z + z}{2 \Delta_i} \right) \right]. \quad (3)$$

In Eq. (3) X_0 describes the probability of finding an Al atom on a group-III site in the unimplanted barrier layer ($X_0 = 0.3$), L_z is the QW width, z is the distance from the QW center along the growth direction, and Δ_i is the interface diffusion length given by

$$\Delta_i = \sqrt{D_v \tau_v V_0} = L_v \sqrt{V_0}, \quad (4)$$

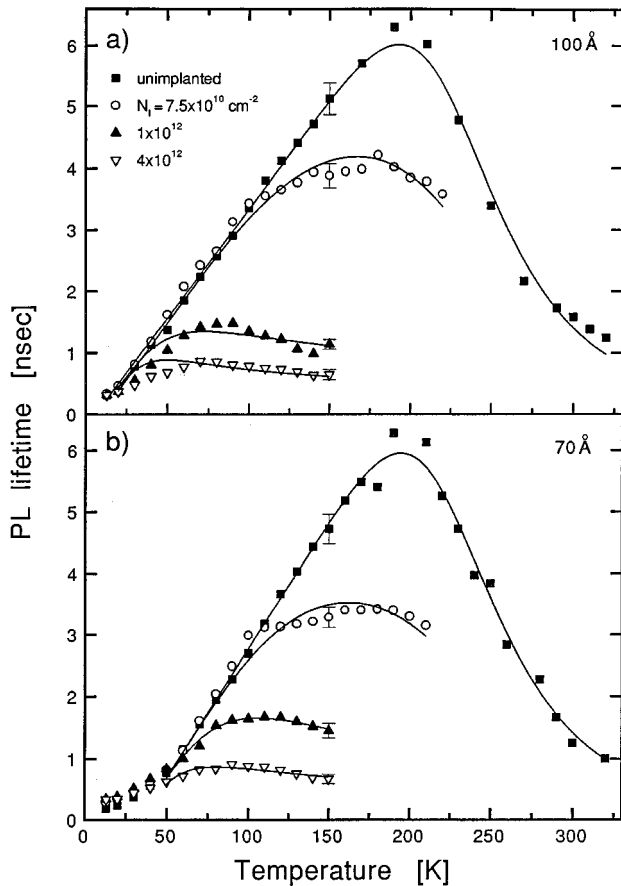


FIG. 4. Temperature dependence of the PL decay times for the unimplanted and implanted 100-Å (a) and 70-Å (b) QW's. The solid curves represent best fits to the experimental data, as discussed in the text.

where L_v is the vacancies diffusion length. V_0 can be estimated from the known implantation dose N_I , the unit-cell volume Ω , and the linear density of vacancies that a traversing ion creates along its track V_ξ :

$$V_0 = V_\xi \Omega N_I. \quad (5)$$

Using Monte Carlo simulations (TRIM 91), we find that V_ξ is about two vacancies per Å along the track of an implanted Bi ion in the QW's region. For the critical implantation dose of $N_c = 7.5 \times 10^{10} \text{ cm}^{-2}$ this yields V_0 of roughly 0.3%.

We can estimate the vacancy diffusion length L_v from the optical spectra as follows. The modifications to the potential structure due to the ion implantation and thermal annealing are reflected in the optical transition energies as measured by both PL and PLE as shown in Fig. 1. For implantation doses below the critical dose N_c , large areas within the QW layer plane remain unaffected. Excitons scatter quickly to these regions which are larger than the two-dimensional (2D) excitonic area. These unaffected areas determine the potential which the recombining exciton "feels," and hence the measured optical transitions are the same as those of the unimplanted QW. For implantation doses which are larger than N_c , no such large enough areas can be found anymore. Everywhere within the QW layer an exciton is in a potential modified by the diffused Al atoms, and thus the optical transitions shift towards higher energies. From the 2D exciton

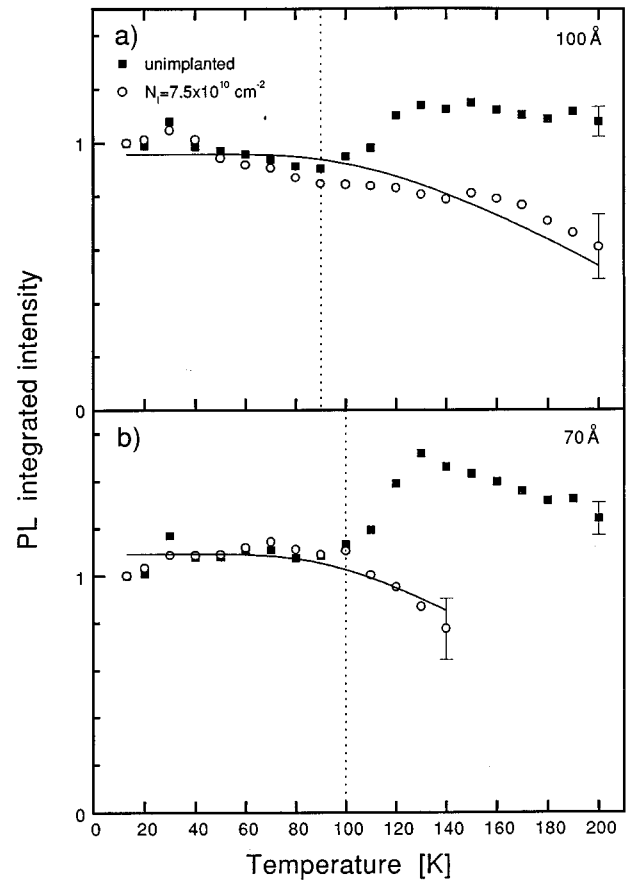


FIG. 5. Temperature dependence of the spectrally integrated PL intensity for unimplanted (solid squares) and implanted by 7.5×10^{10} ions per cm^2 (open circles) 100-Å (a), 70-Å (b) QW's. The solid curves represent best fits to the experimental data, as discussed in the text. The dashed vertical lines mark the experimental critical temperatures as deduced from Fig. 4.

radius (~ 100 Å) and the average distance between neighboring ion tracks at the critical dose, we estimate that the radius of the intermixed area around a single-ion track after the thermal treatment is about 180 Å. This gives a good estimation for the vacancy lateral diffusion length L_v , and is in agreement with Refs. 8 and 10.

We used the PLE spectra of the implanted QW's to independently estimate the interface diffusion length Δ_i in the following way: From the concentration profile given by Eq. (3) the modified potential shape can be easily calculated for any Δ_i (Ref. 14). We then used a transfer-matrix algorithm to calculate energy levels and allowed optical transitions between these levels in the error-function QW as a function of the interdiffusion length Δ_i . The exciton binding energy¹⁵ was added to our calculations neglecting its variation with the QW shape.¹⁶ In the inset to Fig. 6 we depict a typical error-function QW potential structure and a few of its calculated excitonic energy levels. The calculated energies of all the allowed heavy-hole excitonic transitions in a 100-Å (200-Å) error-function QW as a function of interdiffusion length Δ_i are given by the dotted (solid) lines in Fig. 6. The measured optical transitions (from PLE spectra such as shown in Fig. 1) are displayed in Fig. 6 by the empty (full) symbols. The interface diffusion length Δ_i for each implantation dose was chosen to best fit the calculated optical tran-

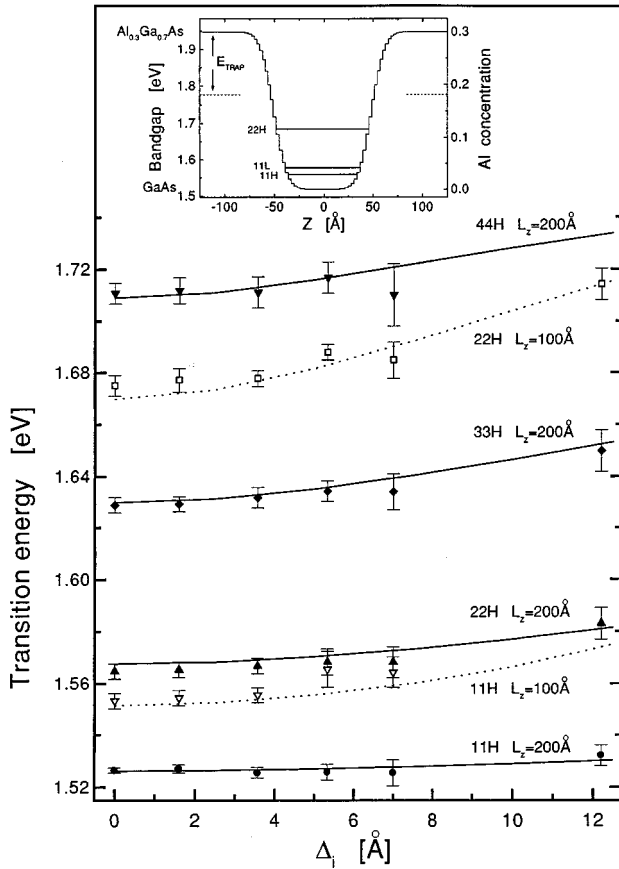


FIG. 6. Calculated heavy-hole excitonic transitions as a function of the interdiffusion length for the 100-Å QW (dashed lines) and the 200-Å QW (solid lines). The PLE measured transitions are represented by the empty symbols for the 100-Å QW and by the full symbols for the 200-Å QW. We use this figure to correlate between the interdiffusion length and the implantation dose (see text). The inset displays the implanted QW Al profile as calculated by Eq. (3) ($L_z = 100$ Å, $\Delta_i = 12$ Å). Few discrete excitonic levels are also shown in the resulted potential structure.

sitions to the measured values. This yields a procedure for relating an interface diffusion length to each implantation dose. For instance, we find $\Delta_i \approx 2.5$ Å (one monolayer) for the critical dose $N_c = 7.5 \times 10^{10}$ cm⁻².

During the annealing process, vacancies and interstitials diffuse laterally from their initial cylindrical source around the ion tracks, until mutual annihilation occurs at a typical time τ_v . The final lattice arrangement deviates from the initial one only near the interfaces due to the gradient of group-III atoms across them. We find the ratio between the interface diffusion length Δ_i and the lateral diffusion length L_v to be of the same order as the square root of V_0 , as expected from Eq. (4). For instance, $\Delta_i/L_v \approx 0.015$, while $\sqrt{V_0} \approx 0.05$ for the critical implantation dose $N_c = 7.5 \times 10^{10}$ cm⁻².

Figure 7 displays the interface diffusion length Δ_i as a function of the implantation dose N_I , as estimated from our PL and PLE measurements using the procedure described above. We have applied the same procedure to the PL data of Allard *et al.*¹¹ and the relevant Δ_i are also presented in Fig. 7 (open circles). The straight solid line in Fig. 7 represents the best fitted power law model to our data yielding $\Delta_i \sim N_I^{1/3}$. We note that the interdiffusion length depends on implanta-

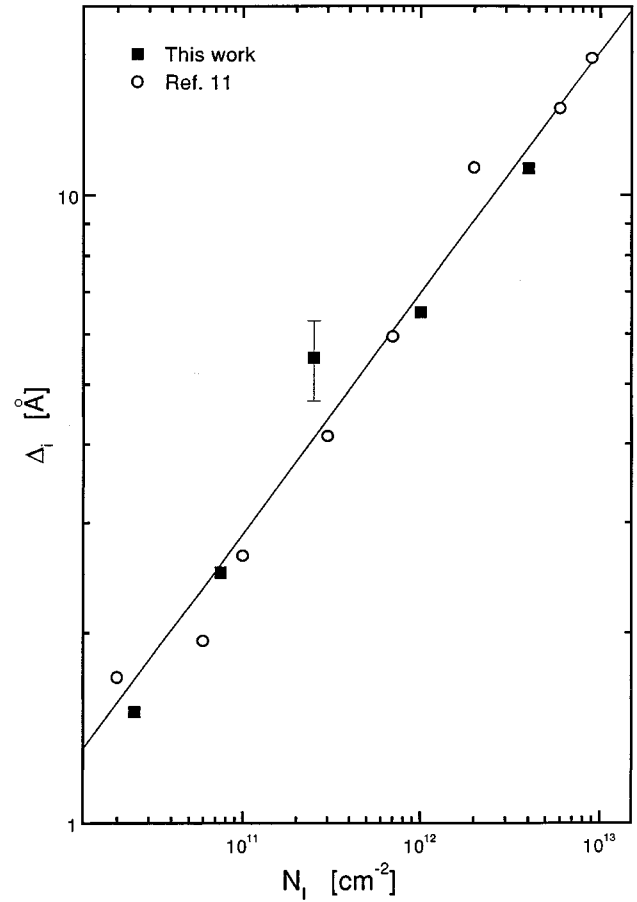


FIG. 7. Interface diffusion length as a function of the implantation dose, as inferred from Fig. 6 (solid squares) and from Ref. 11 (open circles). The solid line represents the best fit to the experimental data, as discussed in the text.

tion dose as a cube-root instead of a square-root dependence which is expected from Eqs. (4), (5) above. The functional dependence of Δ_i on the implantation density found here disagrees with our model description. Clearly, the assumptions on which this conventional model is based¹³ do not adequately describe the physical behavior. Without an attempt to more accurately solve Eqs. (1) and (2), which is beyond the scope of this work, we note, however, that our experimental data suggests that τ_v varies like $V_0^{-1/3}$. This makes sense, since once the average distance between implantation tracks is smaller than the vacancies diffusion length, their lifetime is expected to be proportional to the distance between neighboring vacancies.

To better understand the decay processes of photoexcited excitons in the implanted QW's, one must consider first unimplanted QW's. The PL decay time from various unimplanted QW's is given in Fig. 2 as a function of the lattice temperature, which is also the excitons temperature since their thermalization is considerably faster than their decay.¹⁷ At low temperatures, the excitons are localized in islands within the QW layer, due to interface roughness and width fluctuations. The narrower the well is, the deeper are these localization centers.¹⁸ Thus, at these temperatures and for narrower QW's, the PL decay time is temperature independent,¹⁹ as can be clearly seen in Fig. 2. At higher temperatures, the PL decay times vary linearly with tempera-

ture. This is characteristic of free excitons in a 2D system.¹⁹ At yet higher temperatures (~ 150 K), depending on the QW width, when excitons are activated to energies above the QW potential barrier, the PL decay time decreases, reaching ~ 1 ns at room temperature.

We follow the model of Michler *et al.*²⁰ for a quantitative analysis of the data presented in Fig. 2. This model assumes that at low temperatures excitons recombine radiatively with a characteristic, linearly temperature-dependent lifetime:¹⁹ $\tau_R \sim T$. At high temperature a nonradiative decay channel via barrier states with a temperature-independent lifetime: τ_{NR} is activated. Thermal equilibrium between the lowest electron and hole states in the QW and in the barriers is assumed. This yields an effective temperature-dependent QW excitonic population lifetime τ_{eff} , given by²⁰

$$\tau_{eff}(T) = \frac{1}{\frac{1}{\tau_R(T)} + \frac{1}{\tau_{NR}} \sqrt{CT}^{1/2} \exp\left(-\frac{E_B - E_{11H}}{2k_B T}\right)}, \quad (6)$$

where E_B is the band-gap energy of the barrier, E_{11H} is the energy of the lowest excitonic state in the QW, and $C \sim L_z^2$ is a constant originating from the exciton density of states in the QW and in its barrier.

The solid lines in Fig. 2 show the fits of Eq. (6) to the experimental results. $E_{11H}(L_z)$, $C(L_z)$ and the proportionality constant between τ_R and T were calculated for each QW and only τ_{NR} was used as a single fitting parameter for all the QW's. The value that we obtained for τ_{NR} ($\cong 3$ ps) is in agreement with the directly measured lifetime of barrier states in GaAs/Al_xGa_{1-x}As QW's.²¹

From the known ratio between τ_R and τ_{eff} the temperature dependence of the PL efficiency can be readily calculated since $I_{PL} \sim \tau_{eff}/\tau_R$. The solid curves in Fig. 3 describe our model fitting to the temperature dependence of the spectrally integrated cw luminescence intensities (I_{PL}) from the unimplanted QW's. As can be clearly judged from Fig. 3 our model describes quite adequately the PL intensity quenching at high temperatures, when the nonradiative recombination channels for excitons in the Al_xGa_{1-x}As barriers become gradually available. The model does not account well for the efficiency rise at moderate temperatures (~ 100 K). We suspect that this unexpected phenomena is due to carrier transfer between neighboring wells in these samples.

Having established a model for the unimplanted QW's, we now turn again to the implanted ones. From the dependence on temperature of the PL decay time and efficiency as shown in Figs. 4 and 5, respectively, it is clearly that the implantation increases the nonradiative decay at high temperatures. These nonradiative recombination centers survive the thermal annealing and affect the PL even afterwards. We thus add a nonradiative implantation-induced trap to our model. We assume a finite 2D density of identical nonradiative traps N_{trap} with a recombination lifetime τ_{trap} and energy E_{trap} below the Al_{0.3}Ga_{0.7}As band gap. We also assume that thermal equilibrium, between these states and the QW and barrier states, is reached much faster than the effective excitonic populating decay rate. Under these assumptions, the PL decay time of an implanted QW, τ_{imp} , is given by the following expression:

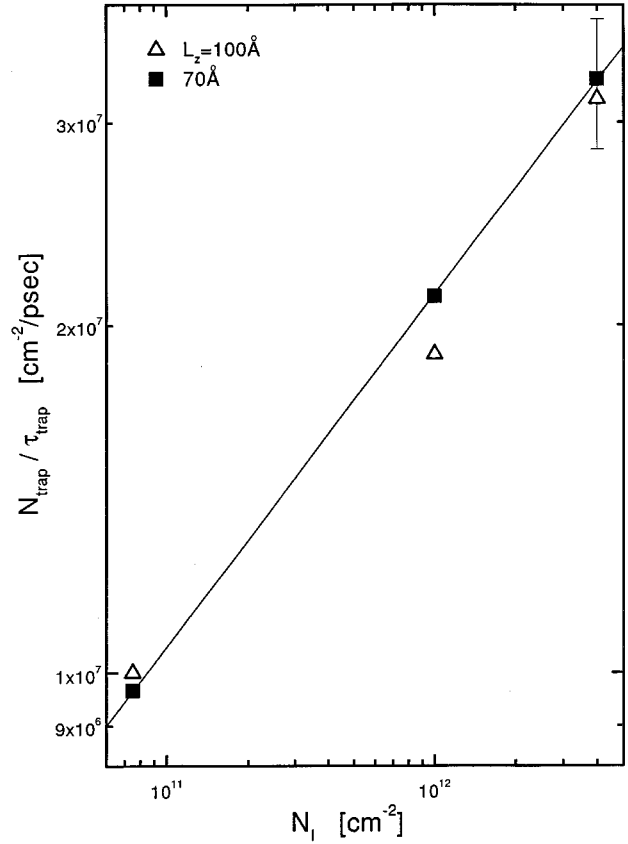


FIG. 8. The fitted parameter N_{trap}/τ_{trap} [see Eq. (7)] as a function of implantation dose for the 100-Å (open triangles), 70-Å (solid squares) QW's. The solid line represents the best fit to the experimental data, as discussed in the text.

$$\tau_{imp}(T) = \frac{1}{\frac{1}{\tau_{eff}(T)} + \frac{N_{trap}}{\tau_{trap}} \frac{1}{N_0} \exp\left(-\frac{E_{trap} - E_{11H}}{k_B T}\right)}. \quad (7)$$

Here τ_{eff} is the PL decay time of the unimplanted QW as given by Eq. (6) taking into account the effect of the implantation-induced structural changes on E_{11H} , and N_0 is the areal density of photoexcited excitons. From the known laser beam power, repetition rate, and spot size, assuming 1% absorption within the QW planes and Al_xGa_{1-x}As barriers, we estimate that $N_0 = 1.3 \times 10^{10} \text{ cm}^{-2}$.

The solid lines in Fig. 4 represent the fitting of τ_{imp} to the experimental decay times in the implanted QW's. In Fig. 5 we fit the PL efficiency: $I_{imp} \sim \tau_{imp}/\tau_R$ to the spectrally integrated cw luminescence of these QW's. The fitted parameters are E_{trap} which we find to be ≈ 170 meV and the ratio N_{trap}/τ_{trap} found to be in the order of $10^7 \text{ cm}^{-2}/\text{ps}$ and depending, as expected, on the implantation dose.

In Fig. 8 we display the fitted parameter N_{trap}/τ_{trap} as a function of the implantation dose N_I for various QW's. As in Fig. 7, we find here that the density of implantation-induced traps N_{trap} goes approximately like the cube root of the implantation density N_I . From the similarity between the implantation dose dependence of the density of traps and the interface diffusion, both showing a cube-root dependency,

we conclude that the nonradiative traps are associated with the Al atoms that diffused into the GaAs QW during the thermal annealing process.

V. SUMMARY

We have shown here that ion-implantation-induced disordering of semiconductor heterostructures create structural modifications to these heterostructures. These modifications can be quantitatively estimated using optical tools such as PL and PLE spectroscopies. We have found that a simple vacancy-assisted diffusion model which assumes a homogeneous initial distribution of implantation-induced vacancies, and results with an error-function-like composition profile for an implanted QW, is insufficient for explaining the ob-

served implantation dose dependence of the interface diffusion length.

From time-resolved measurements we have concluded that a finite density of nonradiative centers is responsible for the reduction in the efficiency and the lifetime shortening of the PL from the implanted samples. The density of these centers, which survive the thermal treatment, is proportional to the density of Al atoms that have diffused into the GaAs QW during the annealing process.

ACKNOWLEDGMENTS

This work was supported by the Israel Science Foundation administrated by the Israeli Academy of Science and Humanities, and by the Fund for the Promotion of Research at the Technion.

-
- ¹S. M. Sze, *Physics of Semiconductor Devices*, 2nd ed. (Wiley, New York, 1981).
- ²R. Kalish and S. Charbonneau, in *Effect of Disorder and Defects in Ion Implanted Semiconductor: Optical and Photothermal Characterization*, edited by C. Christofides and G. Ghibando, Semiconductors and Semimetals Vol. 46 (Academic, Boston, 1997), Chap. 7.
- ³H. Leier, A. Forchel, B. E. Maile, G. Mayer, J. Hommel, G. Weimann, and W. Schlapp, *Appl. Phys. Lett.* **56**, 48 (1990).
- ⁴F. E. Prins, G. Lehr, M. Burkard, S. Y. Nikitin, H. Schweizer, and G. W. Smith, *Jpn. J. Appl. Phys.* **1** **32**, 6228 (1993).
- ⁵F. Laruelle, P. Hu, R. Simes, R. Kubena, W. Robinson, J. Merz, and P. M. Petroff, *J. Vac. Sci. Technol. B* **7**, 2034 (1989).
- ⁶J. Cibert, P. M. Petroff, G. J. Dolan, S. J. Pearton, A. C. Gosard, and J. H. English, *Appl. Phys. Lett.* **49**, 1275 (1986).
- ⁷M. Bode and A. Ourmazd, *J. Vac. Sci. Technol. B* **10**, 1787 (1992); M. Bode, A. Ourmazd, J. A. Rentschler, M. Hong, L. C. Feldman, and J. P. Mannaerts, in *Beam-Solid Interactions: Physical Phenomena*, edited by J. A. Knapp, P. Borgesen, and R. A. Zuhr, MRS Symposia Proceedings No. 157 (Materials Research Society, Pittsburgh, 1989), p. 197.
- ⁸R. Kalish, L. C. Feldman, D. C. Jacobson, B. E. Weir, J. L. Merz, L.-Y. Kramer, K. Doughty, S. Stone, and K.-K. Lau, *Nucl. Instrum. Methods Phys. Res. B* **80/81**, 729 (1993).
- ⁹C. Vieu, M. Schneider, G. Benassayag, R. Paniel, L. Birotheau, J. Y. Marzin, and B. Descouts, *J. Appl. Phys.* **71**, 5012 (1992).
- ¹⁰R. Kalish, L.-Y. Kramer, K.-K. Law, J. L. Merz, L. C. Feldman, D. C. Jacobson, and B. E. Weir, *Appl. Phys. Lett.* **61**, 2589 (1992).
- ¹¹L. B. Allard, G. C. Aers, P. G. Piva, P. J. Poole, M. Buchanan, I. M. Templeton, T. E. Jackman, S. Charbonneau, U. Akano, and I. V. Mitchell, *Appl. Phys. Lett.* **64**, 2412 (1994).
- ¹²S. Alexander, Y. Rabin, and R. Zeitak, *J. Chem. Phys.* **95**, 2012 (1991).
- ¹³J. Cibert, P. M. Petroff, D. J. Werder, S. J. Pearton, A. C. Gosard, and J. H. English, *Appl. Phys. Lett.* **49**, 223 (1986).
- ¹⁴C. Bosio, J. L. Staehli, M. Guzzi, G. Burri, and R. A. Logan, *Phys. Rev. B* **38**, 3263 (1988).
- ¹⁵L. C. Andreani and A. Pasquarello, *Superlatt. Microstruct.* **5**, 59 (1989); *Europhys. Lett.* **6**, 259 (1988).
- ¹⁶A. T. Meney, *J. Appl. Phys.* **72**, 5729 (1992).
- ¹⁷L. C. Andreani, F. Tassone, and F. Bassani, *Solid State Commun.* **84**, 281 (1992).
- ¹⁸M. Colocci, M. Gurioli, and J. Martinez-Pastor, *J. Phys. (France) IV, Colloq.* **3**, C5 (1993).
- ¹⁹D. S. Citrin, *Phys. Rev. B* **47**, 3832 (1993).
- ²⁰P. Michler, A. Hangleiter, M. Moser, M. Geiger, and F. Scholz, *Phys. Rev. B* **46**, 7280 (1992).
- ²¹B. Deveaud, A. Chomette, D. Morris, and A. Regreny, *Solid State Commun.* **85**, 367 (1993).